CHEMISTRY OF MATERIALS
Article

Chem. Mater. **2010,** *22,* 1933–1942 1933
DOI:10.1021/cm9018106

XAS and GIXRD Study of Co Sites in $CoAl_2O_4$ Layers Grown by MOCVD

Chiara Maurizio,*[,†] Naida El Habra,[‡,¶] Gilberto Rossetto,[‡] Marco Merlini,[§] Elti Cattaruzza,[∥] Luciano Pandolfo,[¶] and Maurizio Casarin*[,¶,⊥,#]

[†]*INFM-CNR, OGG-European Synchrotron Radiation Facility, GILDA-CRG B.P. 220, F-38043 Grenoble France,* [‡]*Istituto di Chimica Inorganica e delle Superfici del CNR 35127 Padova, Italy,* [¶]*Dipartimento di Scienze Chimiche, Università degli Studi di Padova, Padova 35131, Italy,* [§]*European Synchrotron Radiation Facility, B.P. 220, F-38043 Grenoble, France,* [∥]*Dipartimento di Chimica Fisica, Università Ca' Foscari, Venezia 30100,* [⊥]*Istituto di Scienze Molecolari del CNR, Padova 35131, Italy, and, and* [#]*Consorzio Interuniversitario di Scienza e Tecnologia dei Materiali, Firenze 50121, Italy*

Received June 26, 2009. Revised Manuscript Received January 26, 2010

The chemical environment of Co sites in $CoAl_2O_4$ layers grown by metal−organic chemical vapor deposition has been investigated by X-ray absorption spectroscopy (XAS) and X-ray diffraction (XRD). It is shown that the air- or [O_2 + H_2O]-annealing at 500 °C of the layers deposited at low temperature induce a partial crystallization with the formation of $(Co_{1-2\eta}Al_{2\eta})(Co_{2\eta}Al_{2(1-\eta)})O_4$ spinel (η = 0.2−0.27). Nevertheless, slightly more than half of Co remains in an amorphous phase, and XAS data are consistent with the formation of a medium-range ordered Co_3O_4 phase, especially upon air-annealing. Layers grown at higher temperatures (600−650 °C) exhibit a similar but more complex structure, since the presence of an additional medium-range ordered phase (likely, $CoAl_2O_4$) is also revealed. The air-annealing at high temperature (800 °C) generates blue, almost completely crystalline, $CoAl_2O_4$ layers. Optical properties of deposited layers are discussed by referring to the outcomes of structural results. In particular, the optical absorption spectrum results negligibly affected by the presence of the amorphous phase, while absorptions present in the 300−500 nm range, responsible for the green layer color and evident in samples annealed in an oxidizing atmosphere or grown at high temperature, are likely caused by the octahedrally coordinated Co ions of the partially inverted spinel $(Co_{1-2\eta}Al_{2\eta})(Co_{2\eta}Al_{2(1-\eta)})O_4$ phase. Despite the XRD analysis that ultimately demonstrates the presence of octahedrally coordinated Co ions, whose oxidation state in the spinel phase is in majority Co(II), the occurrence of Co(III) species with an octahedral environment cannot be ruled out.

Introduction

Transition metal spinels (MAl_2O_4, with M = bivalent metal) are of great technological interest for a wide range of applications, spanning from semiconductor and sensor technology[1] to heterogeneous catalysis.[2] In this class of materials, an important role is played by cobalt aluminate ($CoAl_2O_4$, the Thenard's blue), which, as consequence of its thermal, chemical, and photochemical stability is widely used as a catalyst.[3] Moreover, its peculiar optical properties led also to its extensive use as color filter for automotive lamps[4] or pigment layer on luminescent materials in optical devices.[5] As required for specific applications in this field, several synthetic routes have been established to produce high-quality $CoAl_2O_4$ thin films, such as sol−gel, citrate−gel,[2] and metal−organic chemical vapor deposition (MOCVD).[6] In this regard, some of us recently demonstrated that high purity $CoAl_2O_4$ layers can be deposited at relatively low temperature

*To whom correspondence should be addressed. E-mail: maurizio@esrf.fr (C.M.); maurizio.casarin@unipd.it (M.C.).

(1) (a) Shimizu, Y.; Arai, H.; Seiyama, T. *Sens. Actuators* **1985**, *7*, 11–22. (b) Insley, R. U.S. Patent US3995184, **1985**.
(2) (a) Zayat, M.; Levy, D. *Chem. Mater.* **2000**, *12*, 2763. (b) Escalona Platero, E.; Otero Arean, C.; Parra, J. *Res. Chem. Intermed.* **1999**, *25*, 187. (c) Otero Arean, C.; Penarroya Mentruit, M.; Escalona Platero, E.; Llabres i Xamena, F.; Parra, J. *Mater. Lett.* **1999**, *39*, 22. (d) Meyer, F.; Hempelmann, R.; Mathur, S.; Veith, M. *J. Mater. Chem.* **1999**, *9*, 1755. (e) Meyer, F.; Dierstein, A.; Beck, C.; Hartl, W.; Hempelmann, R.; Mathur, S.; Veith, M. *Nanostruct. Mater.* **1999**, *12*, 71. (f) Balasubramanian, K.; Krishnasamy, V. *J. Chem. Soc.,Faraday Trans.* **1986**, *1*, 2665. (g) Pepe, F.; Occhiuzzi, M. *J. Chem. Soc. Faraday Trans.* **1994**, *90*, 905. (h) Jacobs, J. P.; Maltha, A.; Reintjes, J. G. H.; Drimal, J.; Ponec, V.; Brongersma, H. H. *J. Catal.* **1994**, *147*, 294–300. (i) Baird, T.; Campbell, J.; Holliman, P.; Hoyle, R.; Huxam, M.; Stirling, D.; Williams, B. P.; Morris, M. *J. Mater. Chem.* **1999**, *9*, 599.
(3) (a) Ji, L.; Tang, S.; Zeng, H. C.; Lin, J.; Tan, K. L. *Appl. Catal., A* **2001**, *207*, 247–255. (b) Walsh, A.; Yan, Y.; Al-Jassim, M. M.; Wei, S.-H. *J. Phys. Chem. C* **2008**, *112*, 12044–12050.
(4) Stangar, U. L.; Orel, B.; Krajnc, M.; Korosec, R. C.; Bukovec, P. *Mater. Tehnol.* **2002**, *36*, 387.
(5) (a) Buxbaum, G. *Industrial Inorganic Pigment*, 1st ed.; VCH: Weinheim, Germany, 1993; (b) Duan, X.; Yuan, D.; Cheng, X.; Sun, Z.; Sun, H.; Xu, D.; Lv, M. J. Phys. Chem. Sol. **2003**, *64*, 1021−1025 and references therein; (c) Merikhi, J.; Jungk, H.; Feldmann, C. *J. Mater. Chem.* **2000**, *10*, 1311. (d) Melo, D. M. A.; Cunha, J. D.; Fernandes, J. D. G.; Bernardi, M. I.; Melo, M. A. F.; Martinelli, A. E. Mater. Res. Bull. **2003**, *38*, 1559−1564 and references therein.
(6) (a) El Habra, N.; Crociani, L.; Sada, C.; Zanella, P.; Casarin, M.; Rossetto, G.; Carta, G.; Paolucci, G. *Chem. Mater.* **2007**, *19*, 3381. (b) Carta, G.; Casarin, M.; El Habra, N.; Natali, M.; Rossetto, G.; Sada, C.; Tondello, E.; Zanella, P. *Electrochim. Acta* **2005**, *50*, 4592.

Published on Web 02/12/2010

(350 °C) by MOCVD from a single-source precursor.[6a] Furthermore, optical properties of layers have been shown to be strongly influenced by the deposition temperature and the annealing conditions. In more detail, layers are blue and amorphous if deposited at low temperature (350−550 °C); they change to green if annealed in air between 500 and 700 °C, and they begin to crystallize at $T > 500$ °C and evolve toward blue, polycrystalline $CoAl_2O_4$ if annealed above 700 °C. Incidentally, if the annealing treatment is carried out in a N_2 atmosphere, no color variation is observed.[6a] Analogous color changes induced by thermal treatments have been observed by several authors;[2a,d,7] furthermore, a color change upon calcination is a well-known phenomenon associated either to an increase of crystallite size, as observed for CdS,[8] or to a change in the Co(II) coordinative environment.[2d]

The blue color of $CoAl_2O_4$ films is usually ascribed to absorption features lying between 500 and 700 nm and involving tetrahedrally coordinated Co(II) ions.[6a,9] At variance to that, the green color, implying an absorption band in the 300−500 nm range, has been tentatively associated to Co(III) ions with an octahedral coordinative environment.[2,7] At the present, only the $CoAl_2O_4$ phase formed at high temperature (>700 °C) has been uniquely identified, while green crystalline phases obtained at lower temperature are still under debate. In relation to that, it has to be remarked that, while in ref 2, both the crystalline structure and the optical absorption features of Co_3O_4 (i.e., absorption bands at 300−500 nm and at 700−800 nm) were observed in case of green samples so that the green color was attributed to the crystalline Co_3O_4, in ref 7, the presence of octahedrally coordinated Co(III) ions has been so far inferred just by referring to optical absorption measurements; to this respect, it has to be remarked that octahedrally coordinated Co(II) ions can also exhibit an absorption band in the 300−500 nm range,[10,11] so that in principle the green color could also be related to Co(II) ions, likely in a partially inverted $(Co_{1-2\eta}Al_{2\eta})(Co_{2\eta}Al_{2(1-\eta)})O_4$ phase.

Two more things have to be stressed before continuing: (i) the X-ray diffraction (XRD) patterns of $CoAl_2O_4$ and Co_3O_4 spinel structures and those of their partial inversions are very similar; (ii) an unambiguous interpretation of XRD outcomes up to now was prevented by a possible texture of the crystalline structure, which could not be excluded, since the recorded XRD data did not allow any average over the crystallites orientation.[6a]

In the present contribution, synchrotron radiation-based techniques, namely, grazing incidence XRD (GIXRD) and X-ray absorption spectroscopy (XAS) performed at the Co K photoelectric absorption edge (hereafter K-edge), have been employed to shed new light into the chemical environment of Co ions in $CoAl_2O_4$ layers grown by MOCVD. In particular, the GIXRD analysis, coupled to a 2D detector, permitted to determine the crystalline phase and the degree of inversion of the spinel structure, while X-ray absorption fine structure spectroscopy (EXAFS), widely recognized as the elective tool to investigate the local structure around specific atomic species independently of any long-range order consideration,[12] provided information on the Co sites in a range up to ~3.5 Å as a function of deposition temperatures and annealing conditions. The EXAFS spectroscopy allows the Co nearest neighbor shell to be probed for both crystalline and amorphous layers, providing structural information complementary to XRD. Furthermore, the X-ray absorption near-edge structure (XANES) analysis gave information on the average oxidation state of the Co atoms. As a whole, GIXRD and XAS evidence allowed us to follow the evolution process of layers toward the polycrystalline $CoAl_2O_4$ layers obtained at high temperature and to look into the relationships between optical absorption features, strongly affected by growing and annealing conditions, and the Co site nature.

Experimental Section

Layer Deposition. Layer depositions were performed in a hot wall, low pressure MOCVD reactor by using $Co[Al(O^iC_3H_7)_4]_2$ as precursor.[6a] Layers have been deposited on fused quartz substrates in an oxidizing atmosphere ($O_2 + H_2O$, hereafter O_2^w, obtained bubbling O_2, 100 sccm, into a distilled H_2O vessel) with temperature ranging from 400 to 650 °C, and by adopting a deposition time of 45 min. A detailed description of the layer deposition procedure has been reported elsewhere.[6a] As previously noted,[6a] layers deposited at low temperature (350−550 °C) exhibit all the same structure and color. After their preparation, layers grown at low temperature (400−500 °C) were exposed to different thermal treatments in air (at $T =$ 500 °C for the sample grown at 400 °C, at $T =$ 800 °C for the sample grown at 500 °C), N_2 (for the sample grown at 400 °C) or O_2^w(i.e., the same atmosphere of the growth process) for the sample grown at 500 °C. The duration of the annealing process was 1 h, while for the sample annealed at 800 °C a 3 h-annealing was performed to induce the almost complete layer crystallization. In the forthcoming discussion, as-grown and annealed samples will be classified by labeling them as @XXX and atmosphere@XXX, respectively, where XXX is in both case a temperature in °C referring to the deposition in the former case and to the annealing in the latter.

Layer Characterization. All layers, ~1.5 μm thick, have been characterized by UV−vis spectroscopy, XAS, and GIXRD. UV−vis spectra have been recorded on a double beam UV500-spectrometer (Spectronic Unicam) operating in transmission mode between 250 and 900 nm, and by using the Vision 32 software.

(7) Stangar, U. L.; Orel, B.; Krajnc, M. J. *Sol−Gel Sci. Technol.* **2003**, *26*, 771.
(8) Henglein, A. *Ber. Bunsen-Ges. Phys. Chem.* **1997**, *11*, 1562.
(9) (a) Belova, I.; Roginskaya, Y. E.; Shifrina, R. R.; Gagarin, S.; Plekhanov, Y. V.; Venevtsev, Y. *Solid State Commun.* **1983**, *47*, 577. (b) Cook, J.; van der Meer, M. *Thin Solid Films* **1986**, *144*, 165. (c) Lever, A. B. P. *Inorganic Electronic Spectroscopy*, 2nd ed.; Elsevier Publisher: Amsterdam, The Netherlands, 1984.
(10) Cava, S.; Tebcherani, S. M.; Pianaro, S. A.; Paskocimas, C. A.; Longo, E.; Varela, J. A. *Mater. Chem. Phys.* **2006**, *97*, 102.
(11) Matteucci, F.; Cruciani, G.; Dondi, M.; Gasparotto, G.; Tobaldi, D. M. *J. Solid State Chem.* **2007**, *180*, 3196.
(12) (a) Rehr, J. J.; Albers, R. C. *Rev. Mod. Phys.* **2000**, *72*, 621. (b) Lee, P. A.; Citrin, P. H.; Eisemberger, P.; Kinkaid, B. M. *Rev. Mod. Phys.* **1981**, *53*, 769.

The synchrotron radiation powder diffraction patterns have been collected on the beamline ID09A[13] (European Synchrotron Radiation Facility-ESRF, Grenoble, France) in grazing incidence geometry, to enhance the scattering signal from the investigated layers. A Mar345 Imaging Plate 2D detector has been used to evidence possible preferential crystallite orientations. Employed wavelength and incidence angle were 0.41 Å (corresponding to 30.2 keV) and ~0.3°, respectively (the critical angle corresponds to ~0.08°). The use of an incidence angle of about 3−4 times the critical one allowed to probe the whole deposited layer without increasing too much the signal from the substrate. Data reduction and analysis have been carried out by means of FIT2D[14a] and GSAS[14b] software packages, where the latter allows, through a Rietveld refinement, to evaluate the Co and Al occupancy of tetrahedral and octahedral sites in the spinel structure.[15,16]

XAS measurements have been performed at the Italian beamline GILDA[17] of the ESRF at the Co K-edge. The X-ray radiation energy was selected by using a monochromator equipped with a couple of (311) Si crystals; these crystals were chosen to keep the energy resolution of the X-ray probe (about 0.5 eV) below the natural 1s core-hole width (1.33 eV[18]), that is especially desirable to investigate the pre-edge features of the X-ray absorption spectrum; the harmonics rejection has been achieved by two Pd-coated mirrors working at an incidence angle of 3 mrad. All the samples have been cooled at 80 K to limit thermal vibrations.

Even though XAS measurements have been always carried out in fluorescence mode by employing a photodiode, preliminary data on a series of reference systems (metallic Co, Co-$(C_5H_7O_2)_3$ ($C_5H_7O_2$ = acetylacetonate), and polycrystalline powders of CoO, $CoAl_2O_4$, and Co_3O_4) have been collected in transmission mode to get reference spectra for specific Co coordinative environments. Actually, the Co_3O_4 normal spinel structure[16] contains Co(II) and Co(III) ions tetrahedrically and octahedrally coordinated to oxide ions, respectively; while Co ions have an octahedral environment in both CoO (Co(II)) and $Co(C_5H_7O_2)_3$ (Co(III)). Since the energy scale can slightly shift (usually of less than 0.5 eV) between two subsequent XAS scans because of monochromator instabilities, a XANES spectrum of a Co metallic foil was recorded in parallel with each XANES spectrum of the standard compounds, using two other ionization chambers: this allowed a precise calibration of the energy scale for each spectrum. This procedure was unfeasible for the deposited layers because of the too low transparency of the thick sample substrates; in this case, we have recorded two XANES spectra from a Co foil, one immediately before and the other after the XANES spectrum of each deposited layer. This procedure was repeated 2−4 times for each deposited layer, in order to obtain at least two XANES spectra for each sample recorded in between two Co XANES spectra exhibiting the same edge energy. The analysis of the EXAFS spectra has been performed by using the FEFF8-FEFFIT 2.98 package.[19] The value of the S_0^2 parameter in the standard EXAFS formula[12a] has been determined by referring to the CoO spectrum, while the analysis of the crystalline standard compounds has been achieved through a multiparameter fit in the R space of the k^3-weighted EXAFS spectra (R ranging between 1 and 3.6 Å). The fitting procedure in the k-space led to the same results. Amplitudes and phases for all the single and multiple scattering contributions to the EXAFS signal have been obtained by applying the FEFF8 code to a cluster (radius = 4.4 Å) of the corresponding crystalline phase. Fits of the standard compounds, obtained by using a multiple scattering approach, resulted particularly useful to test the scattering phases and the amplitudes calculated with the FEFF8 code on our experimental data. Amplitude of EXAFS signals have been further corrected for self-absorption effects as indicated in ref 20 (correction less than 6%).

As a first step, the EXAFS analysis has been performed on the first shell of atoms around Co (Co−O coordination) by employing the backscattering amplitude and phase shift evaluated for a $CoAl_2O_4$ cluster. The analysis has been then extended to the range of 1−3.6 Å for all the samples showing a signal from further coordination shells. Such a procedure accounted for the presence of one amorphous phase (a Co−O coordination) and of a linear combination of the partially inverted crystalline spinel $(Co_{1-2\eta}Al_{2\eta})(Co_{2\eta}Al_{2(1-\eta)})O_4$ revealed by the XRD analysis and different medium-range ordered (MRO) phases, i.e. noncrystalline structures providing a contribution to the Fourier transform of the EXAFS signal up to at least R = 4 Å: the MRO phases considered are Co_3O_4 and $CoAl_2O_4$. It has to be remarked that the use of a multiphase approach was mandatory to fit the experimental data for the green layers, that could not be properly simulated by a single phase: the tentative fit with only one phase among $(Co_{1-2\eta}Al_{2\eta})(Co_{2\eta}Al_{2(1-\eta)})O_4$, $CoAl_2O_4$, or Co_3O_4 failed, as later discussed.

To reduce the number of fitting parameters employed for the EXAFS analysis, only an isotropic expansion/contraction of the layer structure has been allowed for each MRO phase. Moreover, as far as Debye−Waller factors are concerned, only that pertinent to the first Co−O coordination has been considered a free parameter, while those of successive shells have been forced to be proportional to the factor of the first one with the same proportionality determined by the EXAFS analysis for the corresponding standard compound. With these constraints, the degrees of freedom in the fit, according to the Nyquist theorem for EXAFS[21] were 6 or higher and the fit quality good (the fractional misfit R[22] was 1−3%, depending on the sample).

3. Results and Discussion

Optical Absorption. The optical absorption spectra of the investigated layers (see Figure 1) are all characterized

(13) http://www.esrf.fr/UsersAndScience/Experiments/DynExtrCond/ID09A/.
(14) (a) Hammerslay, A. P.; Svensson, S. O.; Thompson, A.; Graafsma, H.; Kvick, A.; Moy, J.-P. *Rev. Sci. Instrum.* **1995**, *66*, 2729. (b) Larson, A. C.; Von Drele, R. B. *General Structure Analysis System (GSAS)*; Technical Report, Los Alamos, U.S.A., 1994.
(15) Spinels are double oxides whose formula unit is $[A_{1-2\eta}B_{2\eta}]_T[A_{2\eta}B_{2(1-\eta)}]_OO_4$ with subscripts T and O referring to the tetrahedral and octahedral environment of A and B cations. The spinel unit formula contains eight formula units $\{[A_{1-2\eta}B_{2\eta}]_T[A_{2\eta}B_{2(1-\eta)}]_OO_4\}_8$; moreover, the so-called normal spinel consists of a cubic close packed array of oxide ions with A^{2+} (B^{3+}) ions occupying one-eighth (one-half) of the 64 tetrahedral (32 octahedral) holes in the oxygen lattice (η = 0); while, in the inverse structure (η = 0.5), A and half of B ions change their coordinative environment.
(16) West, A. *Basic Solid State Chemistry*; John Wiley & Sons: Chichester, U.K., 1988.
(17) D'Acapito, F.; et al. *ESRF Newslett*. **1998**, *30*, 42.
(18) Krause, M. O.; Oliver, J. H. *J. Phys. Chem. Ref. Data* **1979**, *8*, 329.
(19) (a) Ankudinov, A.; Ravel, B.; Rehr, J. J.; Newville, M. *Feffit Manual within the Feff Project*; University of Washington: Seattle, WA, 1992−1999; (b) Ankudinov, A.; Ravel, B.; Rehr, J. J.; Conradson, S. D. *Phys. Rev. B* **1990**, *56*, 7565.
(20) Pfalzer, P.; Urbach, M.; nad Klemm, J. P.; Horn, S.; denBoer, M. L.; Kirkland, J. P. *Phys. Rev. B* **1999**, *60*, 9335.
(21) Stern, E. A. *Phys. Rev. B* **1993**, *48*, 9825.
(22) Error reporting recommendations: A report of the standards and criteria committe from the International XAFS Society Standards and Criteria Committee, **2000**.

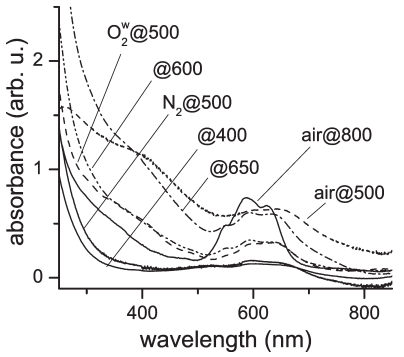

Figure 1. UV−vis absorption spectra of the MOCVD-deposited samples; the solid lines indicate the blue samples, with the others being green.

by the presence of a specific absorption feature in the region 500−700 nm responsible of the blue component of the layer color. The relative intensity of such a feature, usually ascribed to the presence of tetrahedrally coordinated Co(II) ions,[6a,9] varies significantly along the investigated series, being nothing more than a faint signal for layers @400 and N_2@500, but appearing very strong for the sample annealed at the highest temperature (air@800). In this regard, it is worthwhile to mention that both the layer thicknesses and the Co concentration of samples treated at low temperatures are quite similar. In addition to the 500−700 nm feature, all the green layers exhibit an absorption band in the range 300 − 500 nm, tentatively associated by Stangar et al. to Co(III) ion with an octahedral environment.[7]

Grazing Incidence X-ray Diffraction. The X-ray diffraction patterns of the sample deposited at the lowest temperature (@400, not shown) indicates that the deposited layer is amorphous, in agreement with El Habra et al.[6a] The same result is obtained for the sample annealed in N_2 at low temperature (N_2@500). All the other investigated layers are partially crystallized: the GIXRD pattern of the representative @650 (see Figure 2a) consists of uniform diffraction rings indicating the random orientation of crystallites. Very similar results have been obtained for all the samples and, accordingly, they are not herein reported. It is worth noting that the presence of a crystalline structure was already observed in similar layers,[6] but in that case the use of a pixel detector could not establish the random orientation of the crystallites, and so any analysis based on the peaks intensity was prevented. The radial integration of the 2D pattern is displayed in Figure 2b, where the diffraction peaks of @650 are superimposed to the scattering signal deriving from the amorphous silica substrate. The integrated XRD patterns after the background subtraction are reported in Figure 3: all patterns have been indexed with a single spinel phase; in no case, peak splitting or additional diffraction peaks were observed, even at high diffraction angles, indicating that mainly only one crystalline phase is present. The absence of preferential orientation of the crystallites and the high signal-to-noise ratio allowed to perform a Rietveld refinement[23] of the

(23) Young, R. A. *The Rietveld method*; Oxford University Press: Oxford, U.K., 2002.

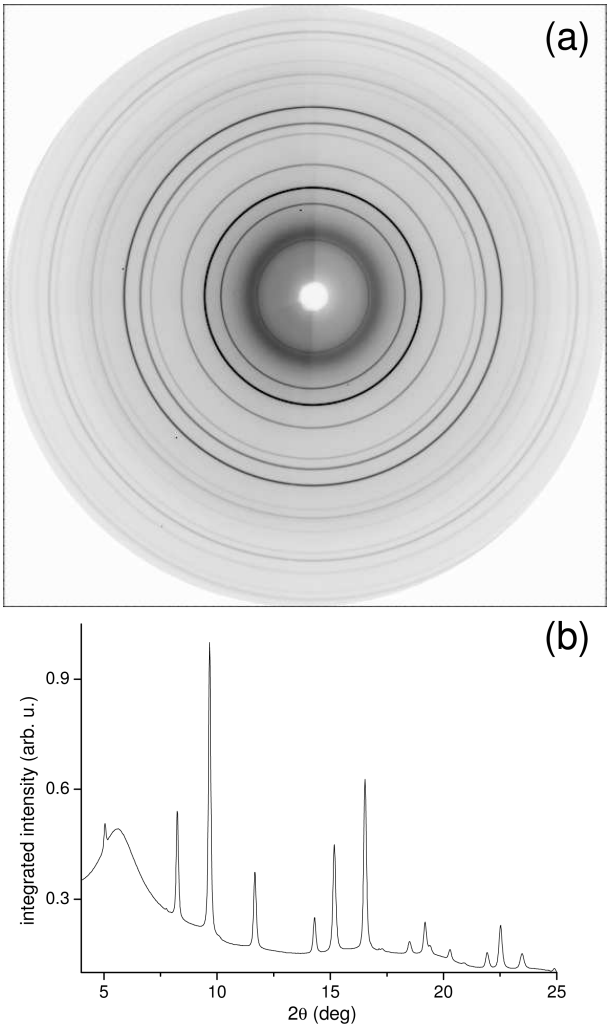

Figure 2. (a) Grazing incidence X-ray diffraction pattern from the sample @650: the sample was mounted vertically and partially shadowed the scattered radiation on the right-hand side of the pattern (the horizon line of the sample surface is vertical and slightly visible in the central part of the pattern); together with the diffraction from the deposited layer, the X-ray scattering from the amorphous silica substrate is also visible. (b) Example of the radially integrated diffracted intensity (sample @650).

spinel structure; it is worth noting that the only way to fit the experimental data for the green layers was to admit a copresence of Co and Al ions in both tetrahedral and octahedral sites of the spinel structure; in particular, the XRD data were found noncompatible neither with the Co_3O_4 structure alone, nor with the $CoAl_2O_4$ one. It was found that a $(Co_{1-2\eta}Al_{2\eta})(Co_{2\eta}Al_{2(1-\eta)})O_4$ spinel phase alone well reproduced the experimental data, without need to include any other phase (for example Co_3O_4) or other stoichiometry of the spinel phase. In particular, the presence of Co_3O_4, if any, is below the significance limit (in tentative fit with a linear combination of $(Co_{1-2\eta}Al_{2\eta})$-$(Co_{2\eta}Al_{2(1-\eta)})O_4$ and Co_3O_4 phases the fraction of Co_3O_4 resulted of few molar percent and did not improve significantly the fit quality). So, the Rietveld refinement allowed estimation of the degree of inversion of the $CoAl_2O_4$ spinels, that is reported in Table 1, together with the refined oxygen occupancy; the best fitting curves are compared to the experimental data in Figure 3. It is worth mentioning that a similar fit quality of the XRD

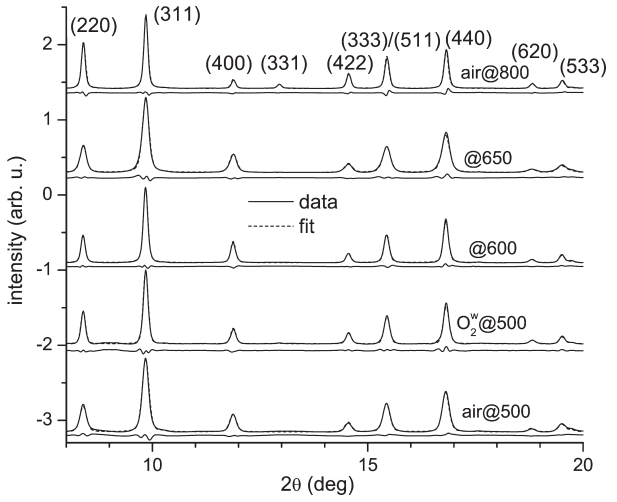

Figure 3. Radially integrated and background-subtracted X-ray diffraction patterns from $CoAl_2O_4$ deposited layers and relative fits; the residue is shown for each spectrum, and the diffraction peaks of the spinel phase are labeled.

Table 1. Results of the XRD Analysis for the deposited $(Co_{1-2\eta}Al_{2\eta})(Co_{2\eta}Al_{2(1-\eta)}O_4)$ Layers

sample	Co tetrahedron occupancy (±0.10)	η (±0.05)	O coordinate (±0.001)
air@500	0.56	0.22	0.257
O_2^w@500	0.61	0.20	0.259
@600	0.47	0.27	0.258
@650	0.50	0.25	0.257
air@800	0.88	0.06	0.264

data has also been obtained with a more complex crystalline phase, namely, $(Co_{1-2\eta}Al_{2\eta})(Co_{2\gamma}Al_{2(1-\gamma)})O_4$ ($0 < \eta$, $\gamma < 0.5$), where the tetrahedral and octahedral occupancies were two independent variables: the obtained results on Co/Al ratio were slightly higher but still in agreement with the value of 0.5, foreseen for the $(Co_{1-2\eta}Al_{2\eta})$-$(Co_{2\eta}Al_{2(1-\eta)})O_4$ phase (only @650 seemed to be richer of Co). This means that our analysis proves the presence of octahedrally coordinated Co(II) ions that are naturally present in a partially inverted spinel phase; nevertheless, the occurrence of octahedrally coordinated Co(III) ions in the same structure could not be proved but also could not be completely ruled out. The inspection of Table 1 testifies that air@800 exhibits a spinel phase with a minimum degree of inversion (the Co(II) fraction in tetrahedral sites, f_{Co}, amounts to 0.88 ± 0.10), while all of the other samples are characterized by an intermediate degree of inversion ($f_{Co} = 0.5-0.6$). The significant difference between air@800 and all the other samples is further testified by looking in Table 1 at the refined oxygen coordinate in the unit cell; to this respect, it is worth observing that in $CoAl_2O_4$ single crystals, the oxygen coordinate is smaller for higher inversion parameter, in agreement with the trend of the present results.[24] Finally, we note that, in agreement with previous observations,[6] a partial crystallization of the deposited layers is achieved at low temperature (500 °C) only by annealing in

(24) O'Neill, H. S. C. *Eur. J. Mineral.* **1994**, *6*, 603.

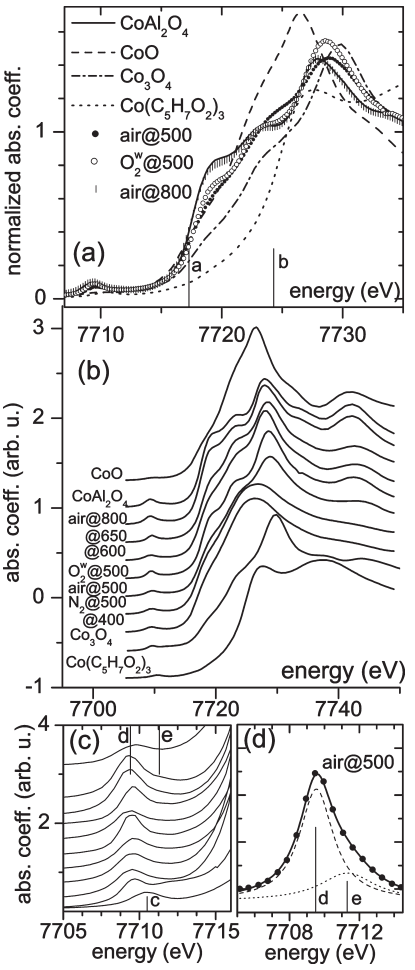

Figure 4. (a) X-ray absorption spectra around the Co K-edge from the standard compounds, compared with that of three representative deposited layers: the marker a indicates the edge energy of the $CoAl_2O_4$ and CoO spectra (maximum of the first derivative); the b indicates the one of the $Co(C_5H_7O_2)_3$ spectrum. (b) XANES spectra from all the samples, compared to those of the standard compounds. (c) Pre-edge X-ray absorption peaks (the order of the spectra is the same as the one in b): the marker c indicates the position of the pre-edge peak for the spectrum of $Co(C_5H_7O_2)_3$; the markers d and e indicate the center of the two pre-edge features of the spectra from the deposited layers, CoO and $CoAl_2O_4$. (d) Fit of the pre-edge peak for a representative spectrum (air@500) with two Lorentzian curves.

oxidizing atmosphere, while a N_2 annealing maintains the original amorphous structure. A possible explanation of this behavior could be an oxygen deficiency in the deposited layers, related to a improper decomposition of the precursor.

These results on the crystalline samples indicate that the blue layer has a $CoAl_2O_4$ structure; for all the green samples, that is, those showing an absorption band in the region of 300−500 nm, the crystalline phase is in agreement with the partially inverted $(Co_{1-2\eta}Al_{2\eta})(Co_{2\eta}$-$Al_{2(1-\eta)})O_4$ spinel.

XANES Analysis. The XANES analysis at Co K-edge was performed to obtain information on the Co oxidation state and on the geometry of the Co site in the deposited layers. In Figure 4(a) the XANES spectra of some Co standard compounds (CoO, $CoAl_2O_4$, $Co(C_5H_7O_2)_3$, and Co_3O_4) are reported. The threshold energies of those compounds containing solely Co(II), that is, CoO and

$CoAl_2O_4$, lie at very close energy value (~7717.3 eV, marker a in Figure 4a); in contrast to that, the absorption threshold of the octahedrally coordinated Co(III) of Co-$(C_5H_7O_2)_3$ is shifted to higher energy (~7724.5 eV, marker b in Figure 4a). The Co_3O_4 spectrum, characterized by 2/3 of octahedrally coordinated Co(III) and 1/3 of tetrahedrally coordinated Co(II) ions has a somehow intermediate behavior, being the absorption edge in between those of $CoAl_2O_4$ and $Co(C_5H_7O_2)_3$ (see Figure 4a). Moreover, the shoulder typical of the tetrahedral coordination (~7719 eV)[25] is well visible for $CoAl_2O_4$ (where Co ions occupy tetrahedral sites) and completely absent in the $Co(C_5H_7O_2)_3$ spectrum, where Co ions occupy octahedral sites. The spectra of some deposited layers (two green and one blue) are superimposed to the standard ones in Figure 4a: the spectrum of air@800 is practically identical to that of $CoAl_2O_4$. The other two, and all of the spectra from the deposited layers, reported in Figure 4b, share with the $CoAl_2O_4$ spectrum the same edge energy, indicating that the most part of Co ions are in the oxidation state (II); moreover, while the spectra of the amorphous samples are pretty smooth and without marked features (apart from the slight shoulder of the tetrahedral coordination, see Figure 4b), suggesting a strongly disordered Co site, the main difference between the spectra of all the green samples (see Figure 4a for two representative cases) and that of $CoAl_2O_4$ is the lower intensity of the shoulder at 7719 eV of the tetrahedral coordination: this suggests that a fraction of Co ions in these layers do not occupy tetrahedral sites. This last observation is in agreement with the GIXRD analysis, that for these green samples indicated that a fraction of Co ions occupy the octahedral sites of the partially inverted $(Co_{1-2\eta}Al_{2\eta})(Co_{2\eta}Al_{2(1-\eta)})O_4$ structure.

The pre-edge region also deserves some comments. The inspection of Figure 4b shows that all the deposited layers exhibit a pre-edge peak, located at ~7709.4 eV, followed by a shoulder at 7711.3 eV (Figure 4c, d). Interestingly, despite the octahedral environment of Co(II) ions in CoO, the energy position of this peak in the CoO spectrum is substantially the same, while it results shifted at higher energies (7710.5 eV) for the octahedral Co(III) ions of $Co(C_5H_7O_2)_3$ (Figure 4c). Parenthetically, we note that the first pre-edge peak is present as well in the Co_3O_4 because of the fraction of Co(II) present in the oxide,[26] while the second broader peak centered at 7711.8 eV for Co_3O_4, is likely related to nonlocal 1s3d transitions.[27,28]

As a whole, the pre-edge features and the threshold energy of the deposited layers indicate that in all the samples the majority of Co is in the oxidation state Co(II) and that in the green samples a fraction of Co ions do not occupy tetrahedral sites.

(25) Kim, M. G.; Yo, C. *J. Phys. Chem. B* **1999**, *103*, 6457.
(26) Shulman, G.; Yafet, Y.; Eisenberger, P.; Blumberg, W. *Proc. Natl. Acad. Sci. U.S.A.* **1976**, *73*, 1384.
(27) Vanko, G.; de Groot, F. M. F.; Huotari, S.; Cava, R. J.; Lorenz, T.; Reuther, M. *arXiv:0802.2744v1*.
(28) de Groot, F.; Vanko, G.; Glatzel, P. *J. Phys.: Condens. Matter* **2009**, *21*, 104207.

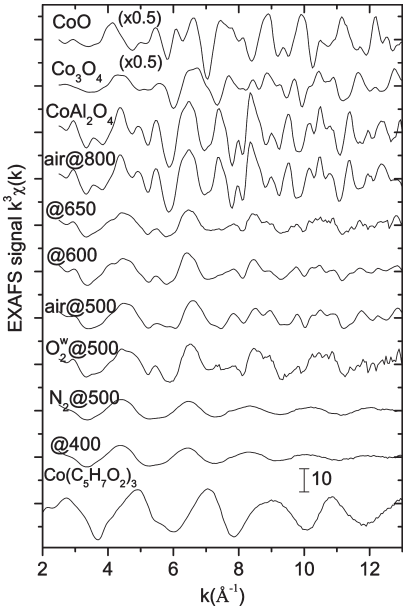

Figure 5. k^3-weighted Co K-edge EXAFS spectra of the investigated samples and standard compounds.

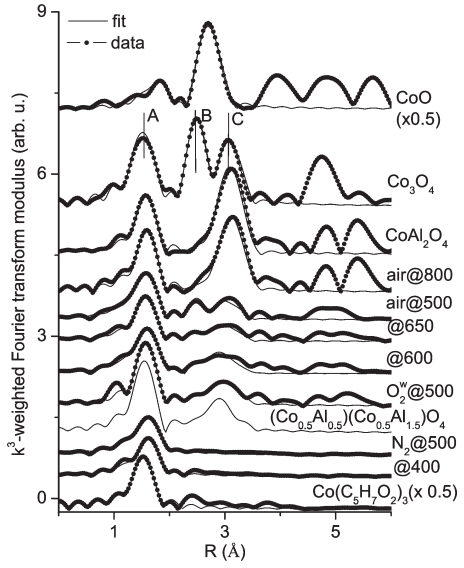

Figure 6. k^3-weighted Fourier transform moduli (in the range 3−12.5 Å^{-1}), and relative fits (in the range R = 1.0−3.6 Å) of the EXAFS spectra in Figure 5. The signal simulated from a partially inverted spinel $(Co_{1-2\eta}Al_{2\eta})(Co_{2\eta}Al_{2\eta(1-\eta)})O_4$ with η = 0.25 is also shown for comparison. The spectra are vertically shifted for clarity, but the relative amplitudes are preserved.

EXAFS Analysis. The EXAFS analysis allowed to investigate the Co site in amorphous phase, as well as to reveal the presence of medium-range-ordered Co-involving phases. Co K-edge EXAFS spectra and their Fourier transform moduli of $CoAl_2O_4$ layers and standard compounds are reported in Figure 5 and Figure 6, respectively; in Figure 6, the simulated Fourier transform modulus of the hypothetical, partially inverted $(Co_{1-2\eta}Al_{2\eta})(Co_{2\eta}Al_{2(1-\eta)})O_4$ (η = 0.25) spinel has been also included for comparison. The corresponding fits are shown in Figure 6 in the R-space and in Figure 7 in the k-space (Fourier-filtered signal) for all the deposited layers, where the signal from the MRO phases that

Table 2. Results of the EXAFS Analysis for the MOCVD Layers and for the Standard Compounds[a]

sample name	amorphous				MRO ($Co_{1-2\eta}Al_{2\eta}$) $0 < \eta < 0.5$		($Co_{2\eta}Al_{2(1-\eta)}$)O_4 $\eta = 0$		MRO Co_3O_4	
	%	N	R(Co−O) (Å)	σ^2 ($\times 10^{-4}$ Å^2)	%	R(Co−O) (Å)	%	R(Co−O) (Å)	%	R(Co−O) (Å)
@400	*100*	4.6 ± 0.4	2.02 ± 0.01	81 ± 4						
N_2@500	*100*	4.0 ± 0.4	2.01 ± 0.01	65 ± 10						
O_2^w500	56 ± 6	2.8 ± 0.7	1.99 ± 0.01	10 ± 8	39 ± 8	1.90 ± 0.02			6 ± 3	1.99 ± 0.02
air@500	55 ± 6	4.0 ± 0.7	2.00 ± 0.01	34 ± 9	26 ± 5	1.89 ± 0.01			19 ± 5	1.93 ± 0.01
@600	57 ± 10	4.8 ± 1.1	2.02 ± 0.02	35 ± 20	21 ± 15	1.90 ± 0.01	15 ± 10	1.91 ± 0.01	7 ± 5	1.99 ± 0.03
@650	73 ± 18	3.3 ± 0.5	1.98 ± 0.02	31 ± 13	7 ± 5	1.89 ± 0.02	13 ± 10	1.90 ± 0.01	7 ± 5	1.96 ± 0.02
air@800	*0−10*	*4−6*	2.00 ± 0.05	21 ± 7			95 ± 5	1.94 ± 0.01		

reference samples	−	N	R (Å)	σ^2 ($\times 10^{-4}$ Å^2)
$CoAl_2O_4$	Co−O	*4*	1.94 ± 0.01	30 ± 15
	(Co−O)	(4)	(1.94)	
Co_3O_4	Co−O	*6*	1.93 ± 0.01	38 ± 5
	Co−O	*4*	1.94 ± 0.01	18 ± 6
	(Co−O)	(6;4)	(1.92;1.93)	
CoO	Co−O	*6*	2.13 ± 0.01	64 ± 14
	Co−Co	*12*	3.02 ± 0.01	52 ± 6
	(Co−O)	(6)	(2.13)	
	(Co−Co)	(12)	(3.01)	
$Co(C_5H_7O_2)_3$	Co−O	5.6 ± 0.3	1.89 ± 0.01	22 ± 5
	(Co−O)	(2;4)	(1.88;1.89)	

[a] *N* is the coordination number, *R* the interatomic distance, and σ^2 the Debye-Waller factor; the parameters in italics were fixed during fitting. Crystallographic values are reported in parentheses for comparison. For the deposited layers, only the first shell parameters (and only the shortest Co−O distance) are reported: as explained in the text, *R* and σ^2 for the interatomic correlations beyond the first one scale as in the EXAFS fitting of the corresponding crystalline structure.

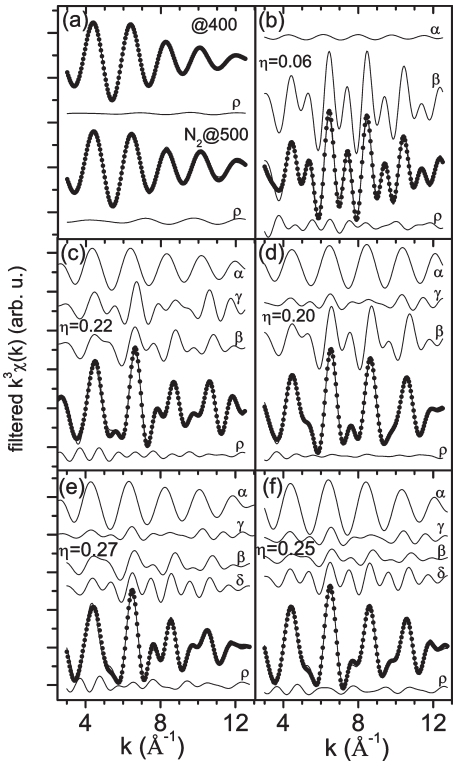

Figure 7. Fourier-filtered signal (markers, in the range 1.0−3.6 Å) of the deposited layers: (a) @400 and N_2@500, (b) air@800, (c) air@500, (d) O_2^w@500, (e) @600, (f) @650. The best fit curves are superimposed to the experimental data; the residual (ρ) as well as all the signals from the medium-range ordered phases that contribute to the fit are reported (α, Co−O amorphous signal; β, ($Co_{1-2\eta}Al_{2\eta}$)($Co_{2\eta}Al_{2(1-\eta)}$)O_4; γ, Co_3O_4; δ, $CoAl_2O_4$).

contributed to the fit are also displayed. Fits of the Fourier transform moduli were limited to the first shell of neighbors for amorphous samples and extended up to R = 3.6 Å for the others. Finally, results of the fitting procedures for deposited layers and standards are grouped in Table 2.

Focus first on the Fourier transform moduli of the standard compounds, specifically, CoO, $CoAl_2O_4$, and Co_3O_4 (Figure 6). The peak **A** is due to a Co−O coordination: its position is the same for $CoAl_2O_4$ and Co_3O_4 spectra, while is shifted at higher *R*-value for CoO (correspondingly, the Co−O first shell distance is about 1.95 Å in the first two, while is 2.13 Å in CoO). Furthermore, the signal in the range R = 2−4 Å is strongly affected by the structure. In more detail, the Fourier transform of the Co_3O_4 spectrum exhibits, beside the **A** feature, two further peaks (**B** and **C**), the former resulting from the correlation between two adjacent octahedral sites ~2.85 Å apart and so solely caused by Co with an octahedral environment (2/3 of Co ions), the latter taking its main contribution from the scattering between Co ions in tetrahedral and octahedral sites (~3.34 Å aside), and both of them partially enhanced by a focusing effect of the first shell of O atoms around tetrahedral sites.[19a] According to the absence of any Co ions with an octahedral coordination, the Fourier transform modulus of the $CoAl_2O_4$ EXAFS spectrum is characterized, in the range of R = 2−4 Å, by the presence of the single peak **C**. Interestingly, this is the same *R* range for which modifications induced by the partial inversion of the $CoAl_2O_4$ spinel structure in the EXAFS spectrum are particularly evident. More specifically, the coexistence of Co and Al species in octahedral and tetrahedral sites generates, in the partially inverted ($Co_{1-2\eta}Al_{2\eta}$)($Co_{2\eta}Al_{2(1-\eta)}$)O_4 spinel, a broader structure peaked at ~3 Å and well

distinguishable in the FEFF8 simulation reported in Figure 6; it is worth noting that, from a FEFF8-based analysis,[19] both the amplitude and phase of this signal are significantly different from the ones related to the peak at 2.7 Å in the CoO spectrum and those related to the 12-fold Co−Co coordination at 3.01 Å.

Focus now on the EXAFS analysis of the $CoAl_2O_4$ deposited layers. The EXAFS spectrum of the low temperature deposited layer is characterized by the presence of just one damped oscillation (see Figure 5) generated by the first Co−O coordination shell. Accordingly, the Fourier transform modulus exhibits only one coordination peak (**A** in Figure 6), which is well reproduced by a single shell of O atoms around Co ions (see fit in Figure 6 and Figure 7a and results in Table 2); the coordination number is slightly higher than four and the corresponding Debye−Waller factor is significantly higher than that pertinent to all our standards, thus indicating that the high structural disorder is present not only at long range, as testified by XRD, but also locally at the Co site, also in agreement with the indication of the XANES spectrum. So, overall the experimental results (XANES, EXAFS, XRD) indicates that the low temperature deposited layer is amorphous and that the structural disorder involves also the local site of the Co(II) ions.

Effect of Thermal Annealing in Selected Atmospheres. For the sample N_2@500, the first shell EXAFS analysis indicates a 4 oxygen coordination for Co ions. Consistently, with a Co site partial order induced by the thermal annealing, the Debye−Waller factor is lower in N_2@500 than in @400 but still higher than that pertinent to crystalline standard compounds. The absence of any signal from coordination shells beyond the first one is in agreement with the amorphous structure revealed by the XRD analysis. The experimental analyses (optical absorption, GIXRD, XANES, EXAFS) of the sample N_2@500 indicate that it is pretty similar to @400, so that mainly the same conclusions can be drawn.

As far as the layers annealed at 500 °C in oxidizing atmosphere are concerned, the Fourier transform of the EXAFS spectra shows a signal from coordination shells beyond the first one (see Figure 6): this indicates that the oxidizing annealing has induced a partial ordering of the Co site, extending beyond the first shell. Certainly the $(Co_{1-2\eta}Al_{2\eta})(Co_{2\eta}Al_{2(1-\eta)})O_4$ crystalline phase revealed by XRD contributes to this signal; the presence of other medium-range ordered phases is addressed in the following. The EXAFS signal lying in the range $R = 2-3.5$ Å is different for air@500 and O_2^w@500 and is less intense than that of any crystalline standard compound, suggesting that the medium-range ordered phases do not involve the majority of Co ions. In this respect, it has to be highlighted that the shape of the signals pertinent to O_2^w@500 and air@500 samples look like the ones of $(Co_{1-2\eta}Al_{2\eta})(Co_{2\eta}Al_{2(1-\eta)})O_4$ ($\eta = 0.25$) and Co_3O_4, respectively. The quantitative analysis (see Table 2, Figure 6 and Figure 7c, d) indicates that slightly more than 50% of Co ions belong to an amorphous phase with a coordination number of 4 or less (the coordination number is lower in the sample annealed in O_2^w), only contributing to the first Co−O coordination. Furthermore, the EXAFS analysis extended up to $R = 3.6$ Å has shown that a good fit of shells beyond the first one needs contributions not only from the $(Co_{1-2\eta}Al_{2\eta})(Co_{2\eta}Al_{2(1-\eta)})O_4$ crystalline phase ($\eta = 0.20-0.27$. as from XRD) but also from a MRO Co_3O_4 component. In this respect, it can be useful to remind that Co_3O_4 and $(Co_{1-2\eta}Al_{2\eta})(Co_{2\eta}Al_{2(1-\eta)})O_4$ EXAFS signals are significantly different in the $R = 2-4$ Å region. Moreover, the EXAFS analysis indicates that the fraction of Co ions in the $(Co_{1-2\eta}Al_{2\eta})(Co_{2\eta}Al_{2(1-\eta)})O_4$ crystalline phase is the major MRO phase in the O_2^w annealed sample, while the $(Co_{1-2\eta}Al_{2\eta})(Co_{2\eta}Al_{2(1-\eta)})O_4$ percentage is close to the Co_3O_4 one upon annealing in air. Before going on, it has to be remarked that the presence of a crystalline Co_3O_4 phase has been reported in $CoAl_2O_4$ particles prepared by sol−gel[2a] and calcinated at 400 °C. In the present case, the Co_3O_4 is a MRO phase formed upon annealing, likely located in the proximity of (or at the surface of) Al-rich amorphous particles;[2a] moreover, its formation is favored by annealing in a dry oxidizing atmosphere. As previously mentioned, the inspection of the edge energy region proves that the prevalent Co oxidation state is Co(II). This is not in disagreement with the observed presence of Co_3O_4 since the fraction of Co(III) ions involved does not exceed ~15% (see Table 2). Anyway, we have no evidence to exclude that a (minor) part of Co ions in the octahedral sites of $(Co_{1-2\eta}Al_{2\eta})(Co_{2\eta}Al_{2(1-\eta)})O_4$ are in the oxidation state Co(III).

Finally, the EXAFS spectra and the corresponding Fourier transform modulus of the sample annealed at the highest temperature (air@800) is very close to the one of $CoAl_2O_4$ (see Figures 5, 6, and 7b). The quantitative EXAFS analysis indicates that the $CoAl_2O_4$ phase of the air@800, also evidenced by GIXRD, involves most part of Co atoms (see Table 2). Parenthetically, it can be of some interest to point out that a minor Co−O amorphous coordination has been also revealed, but the EXAFS signal generated by the $CoAl_2O_4$ phase was so strong to prevent any precise determination of the amorphous phase coordination number, while other MRO phases were below the EXAFS detectable limit. So, for this sample, XRD, XANES, and EXAFS analyses indicate that, in agreement with previous observations,[6a] the crystalline phase is essentially $CoAl_2O_4$ and it involves most part of the Co species. Moreover, the air@800 Debye−Waller factor is low and comparable with that of the $CoAl_2O_4$ standard compound thus indicating a well ordered structure with most part of the Co(II) ions tetrahedrally coordinated.

As a whole, the main effect of the thermal annealing is that of inducing a progressive ordering of the layers, from a completely amorphous one with disordered tetrahedral Co sites (N_2@500) to an almost completely crystalline $CoAl_2O_4$ layer of sample air@800. At low annealing temperature and oxidizing atmosphere, the polycrystalline spinel phase is in agreement with $(Co_{1-2\eta}Al_{2\eta})(Co_{2\eta}Al_{2(1-\eta)})O_4$, with $\eta = 0.20-0.27$; the crystalline phase is

present together with a medium range ordered Co_3O_4-like phase (samples air@500 and O_2^w@500). The increase of the annealing temperature determines a progressive structural ordering at different levels: (i) long-range ordering, with the increase of the crystalline phase, (ii) ordering of the Co and Al cations in the spinel structure (at high temperature Co occupies tetrahedral sites and Al octahedral ones, while at low temperature the occupation is mixed), and (iii) short-range ordering of the Co site, testified by the decrease of the Debye−Waller factor (see Table 2).

Effect of the Growth Temperature. With respect to the annealed layers, EXAFS results pertaining to the samples grown at high temperature (@600 and @650) indicate a further complex structure. Analogously to air@500 and O_2^w@500, signals from a Co−O amorphous phase and the $(Co_{1-2\eta}Al_{2\eta})(Co_{2\eta}Al_{2(1-\eta)})O_4$ structure were not sufficient to get a good fit of experimental data. In this case, the only way to obtain a reasonable fit was that of admitting the presence of two other MRO phases: Co_3O_4 and, likely, $CoAl_2O_4$ (see Table 2, Figures 6 and 7e, f). Moreover, for both samples, the presence of a CoO slight contribution could not be completely ruled out. In this regard, it has to be noted that the relative percentage of different phases is well-defined only when no more than two MRO components are present (as in the case of air@500 and O_2^w@500), while a higher number of contributions implies a great uncertainty in the relative weight. The complex structure of these layers with respect to the 500 °C-annealed ones could be likely because of the absence of the annealing process; the high temperature of the substrate certainly favors the interdiffusion of the different species during the growth process and likely the beginning of a crystalline ordering; on the other hand, while the first deposited atomic layers remain at the deposition temperature for the most part of the deposition process and so undergo a sort of O_2^w-annealing, the atomic layers closer to the surface, being the last to be deposited, experience this treatment for a shorter time. A certain variety of the structures formed at different depth, with respect to samples first deposited and then annealed, is likely to be expected.

Structural Results and Optical Properties. The structural results obtained with different characterization techniques shed some light on the optical properties of the $CoAl_2O_4$ deposited layers and in particular on the layer color.

The two amorphous layers (samples @400 and N_2@500) exhibit similar structural and optical properties. From the previous considerations, the oxidation state of Co is mainly Co(II) (from XANES), and Co occupies disordered tetrahedral sites (from XANES and EXAFS). Considering the faint optical absorption band of the sample, typical of the tetrahedral coordination (see Figure 1), we can conclude that the layer optical properties are negligibly affected by the amorphous and disordered Co sites.

In contrast to that, consider the sample heated at the highest temperature (air@800): XRD and EXAFS analyses indicate that, in agreement with previous observations,[6a] the crystalline phase is essentially $CoAl_2O_4$, and it involves most part of the Co species. Moreover, the air@800 Debye−Waller factor is low and comparable with that of the $CoAl_2O_4$ standard compound thus indicating a well ordered structure with most part of the Co(II) ions tetrahedrally coordinated and likely responsible for the strong absorption in the range 500−700 nm.

Consider now the green layers, that is, those characterized by an absorption feature at 300−500 nm in addition to the one at 500−700 nm. The XRD data are in agreement with a $(Co_{1-2\eta}Al_{2\eta})(Co_{2\eta}Al_{2(1-\eta)})O_4$ crystalline phase (η = 0.20−0.27), and the XANES analysis indicates that Co remains mainly in the Co(II) oxidation state. EXAFS analysis shows a more complex structure, enlightening that other MRO phases are also present. Focus on the 500 °C-annealed layers, that are composed of an amorphous part (involving slightly more than 50% of Co), plus a crystalline phase ($(Co_{1-2\eta}Al_{2\eta})(Co_{2\eta}Al_{2(1-\eta)})O_4$) and a MRO Co_3O_4 phase. Since the results on the amorphous layers suggest that the amorphous part does not contribute so much to the optical absorption features, we can consider, as a first approximation, only the medium or long-range ordered phases to shed light on the layer optical properties. Since the tetrahedrally coordinated Co(II) mainly contributes to the triplet in the optical absorption spectrum discussed above (500−700 nm), the origin of the absorption band at 300−500 nm should be found in the octahedrally coordinated Co ions. To this respect it is worth noting that a similar band is generated by octahedrally coordinated Co(II);[10,11] on the other hand, Co_3O_4 thin films, normally of brownish color, also exhibit an absorption band in the same region, that is always present together with a second band located in the range 700−800 nm.[29,30] Even in nanostructured Co_3O_4, these two bands are both present at the same time and with comparable intensity.[29] In our case, the second band is absent: this is probably because the Co_3O_4 is in an extremely disordered phase, while the Co_3O_4 optical absorption is very sensitive to the structure of the whole unit cell.[31] This suggests that the origin of the green color (300−500 nm band) is mainly related to the octahedrally coordinated Co (II) ions of the $(Co_{1-2\eta}Al_{2\eta})(Co_{2\eta}Al_{2(1-\eta)})O_4$ crystalline structure. As a final consideration, our analysis does not completely exclude the presence of a minor fraction of octahedrally coordinated Co(III) ions into the $(Co_{1-2\eta}Al_{2\eta})(Co_{2\eta}Al_{2(1-\eta)})O_4$ crystalline structure that, in case, could also also contribute to the 300−500 nm absorption band.

Conclusions

The coordinative environment of Co ions in $CoAl_2O_4$ layers grown by MOCVD has been investigated by

(29) (a) de Julian Fernandez, C.; Mattei, G.; Sada, C.; Battaglin, G.; Mazzoldi, P. *Mater. Sci. Eng., C* **2006**, *26*, 987. (b) Drasovean, R.; Monteiro, R.; Fortunato, E.; Musat, V. *J. Non-Cryst. Solids* **2006**, *352*, 1479.
(30) (a) Barrera, E.; Viveros, T.; Avila, A.; Quintana, P.; Morales, M.; Batina, N. *Thin Solid Films* **1999**, *346*, 138. (b) Pejova, B.; Isahi, A.; Najdoski, M.; Grozdanov, I. *Mater. Res. Bull.* **2001**, *36*, 161.
(31) Miedzinska, K.; Hollebone, B.; Cook, J. *J. Phys. Chem. Solids* **1987**, *48*, 649.

synchrotron radiation-based techniques, namely X-ray absorption spectroscopy and grazing incidence X-ray diffraction. It has been shown that the annealing at 500 °C, in air or in O_2^w, of layers deposited at low temperature induces a partial crystallization with the formation of a $(Co_{1-2\eta}Al_{2\eta})(Co_{2\eta}Al_{2(1-\eta)})O_4$ spinel, with $\eta = 0.20-0.27$. Nevertheless, slightly more than half of Co ions remain in an amorphous phase and the formation of a medium-range ordered Co_3O_4 phase, especially upon air-annealing, is evidenced by EXAFS. Layers grown at higher temperatures (600−650 °C) exhibit a similar but further complex structure since the presence of an additional medium-range ordered phase (likely $CoAl_2O_4$) is also detected. The air-annealing process at high temperature (800 °C) induces an almost complete crystallization with the formation of blue $CoAl_2O_4$ layers. The optical properties of the layers are discussed on the basis of the structural results. The amorphous phase seems to have a minor effect on the optical absorption spectrum: the amorphous layers grown at low temperature (and eventually annealed in N_2 at 500 °C) are pale blue nearly transparent. The progressive ordering of the Co site induced by the air annealing has an effect on the optical absorption. In particular, the 300−500 nm absorption band, responsible for the green color and evident after annealing in oxidizing atmosphere or in the high-temperature grown samples, is likely related to the octahedrally coordinated Co ions of the $(Co_{1-2\eta}Al_{2\eta})$-$(Co_{2\eta}Al_{2(1-\eta)})O_4$ crystalline phase, likely in the oxidation state (II).

Acknowledgment. We warmly acknowledge Francesco D'Acapito of the OGG-CNR (Italian beamline GILDA of ESRF) for fruitful discussions; we acknowledge the European Synchrotron Radiation Facility and the Italian Collaborating Research Group GILDA for the provision of the synchrotron radiation facility. GILDA is a project jointly financed by CNR and INFN.